Proceedings of IMECE'2002
2002 ASME International Adaptive Structures and Materials Systems Symposium
November 17-22, 2002, New Orleans , LA, USA

IMECE02/TTRSP-32942

INTEGRATED PIEZOELECTRIC LINEAR MOTOR FOR VEHICLE APPLICATIONS

Mark Vaughan

Center for Intelligent Material Systems and Structures
310 Durham Hall
Virginia Tech
Blacksburg, Virginia 24061-0261

Donald J. Leo *

Center for Intelligent Material Systems and Structures
307 Durham Hall
Virginia Tech
Blacksburg, Virginia, 24061-0261
donleo@vt.edu

ABSTRACT

The focus of this research was to create a linear motor that could easily be packaged and still perform the same task of the current DC motor linear device. An incremental linear motor design was decided upon, for its flexibility in which the motor can be designed. To replace the current motor it was necessary to develop a high force, high speed incremental linear motor. To accomplish this task, piezoelectric actuators were utilized to drive the motor due their fast response times and high force capabilities.

The desired overall objectives of the research is to create an incremental linear motor with the capability of moving loads up to one hundred pounds and produce a velocity well over one inch per second. To aid the design process a lumped parameter model was created to simulate the motor's performance for any design parameter. Discrepancies occurred between the model and the actual motor performance for loads above 9.1 kilograms (20 pounds). The resulting model, however, was able to produce a good approximation of the motor's performance for the unloaded and lightly loaded cases. The incremental linear motor produced a velocity of 4.9 mm/sec (0.2 in/sec) at a drive frequency of 50 Hz. The velocity of the motor was limited by the drive frequency that the amplifiers could produce. The motor was found to produce a stall load of 17 kilograms (38 pounds). The stall load of the design was severely limited by clearance losses.

INTRODUCTION

Piezoelectric linear motors have been created using a wide variety of different methods. This ability to create a variety of piezoelectric linear motors is due to the versatility a designer has when using piezoelectric ceramics. Piezoelectric ceramics can be purchased in many different shapes and sizes, allowing for flexibility during the design process. This versatility when designing a piezoelectric linear motor has a great advantage over traditional linear motors. As a result many piezoelectric linear motors have been designed with a specific application in mind.

One technique of creating a piezoelectric linear motor uses an inchworm type method of motion. The inchworm type linear motor is known to produce high forces, accurate positioning, and large displacements limited only by the length of the guide channel. These piezoelectric motors can be designed relatively small and light, due to the large force capabilities of piezoelectric ceramic material. One of the most favorable aspects of the inchworm motor is its ability to be integrated into the structure of the mechanical device to be moved. For example, the inchworm motor can be designed to mount in a preexisting guide channel for a mechanical device. The inchworm technique also allows the linear motor to change directions by simply switching the

*Address all correspondence to this author.

clamping cycles. The result is a high force, bi-directional motor that can be easily packaged.

The inchworm motors presented in this survey can be separated by the method in which the large movements are produced. There are basically three different types of actuation techniques. The first technique can be referred to as a "walker", in which the both the extending and the clamping mechanisms moving along a guiding shaft(A.D. Brisbane, 1968; S. Hsu, A. Arbor, and A. Blatter, 1966; G.V. Galutva, 1972; C.G. O'Neill and C.E. Foster, 1980; T. Fujimoto, 1988; B. Zhang and Z. Zhu, 1994; S. Canfield, B. Edinger, M. Frecker, and G. Koopmann, 1999; B. Edinger, M. Frecker, and J. Gardner, 1999). Here the structure appears to be walking along the path of actuation. The second technique can be referred to as a "pusher", in which the extending and clamping mechanisms remain stationary(G.R. Stibitz, 1964; R.A. Bizzigotti, 1975; W.G. May, Jr., 1975; A. Hara, T. Horinchi, K. Yamada, S. Takahashi, and K. Nakamura, 1986; T. Murata, 1990; J.E. Miesner and J.P. Teter, 1994; J. Frank, G. Koopmann, W. Chen, and G. Lesieutre, 1999). Here the structure appears to push the shaft along the path of actuation. The third technique referred to as the hybrid "walker-pusher", in which either the extending or the clamping mechanism moves along the shaft while the other mechanism remains stationary(G.L. Locher, 1967; T. Shibuya, 1988; Galante, 1997; J. Oliver, R. Neurgaoukar, J. Nelson, and C. Bertolini, 1998). An improved inchworm design, called a 'caterpillar' design, was developed by T. Pandell and E. Garcia (1996). The performance of the device claimed a stall load of approximately 20 N and an unloaded speed of 1 cm/sec; however, the improvement over the inchworm technique is the most important result of this design. Micromachining techniques have also been utilized to create miniature inchworm designs with forces in the 1 to 20 N range and speeds on the order of 1 to 13 cm/sec (S. Lee and M. Esashi, 1995; G. Carman, Q. Chen, D. Yao, and C. Kim, 1999).

The goal of this research is to design an inchworm-type motor that can traverse the interior of a channel section. The goal is to develop a motor that maximizes output mechanical power. The paper is organized into a discussion of the design, a modeling section, and a discussion of experimental results.

Motor Design

The present work is based on a conventional inchworm motor design as shown in Figure 1. Inchworm motion requires six steps to produce an incremental displacement Δ. The key design parameters are the material for the braking mechanisms and extending mechanisms. The amount of incremental motion per cycle and the holding force of the

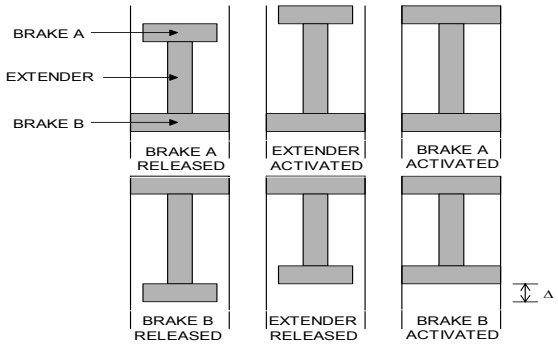

Figure 1. Inchworm-type motors using two brakes and one extending mechanism.

actuator are a function of the parameters that define the brake material and extender material. The decision was made to purchase a compliant amplified actuator for the extending mechanism. Before deciding on an amplified actuator to use, a comparison was conducted to find the actuator that best suited the project. The comparison found two likely actuators that produced characteristics suitable for the project, the APA95ML and APA120ML manufactured by Cedrat Recherche. The performance characteristics for these two actuators are shown in Table 1.

Table 1. Compliant actuator characteristics [Cedrat_Recherche (2000)].

Characteristic	*Unit*	*APA95ML*	*APA120ML*
Displacement	(um)	94	120
Blocked Force	(N)	1900	1400
Stiffness	(N/um)	20.2	11.7
Voltage Range	(V)	-20 to 180	-20 to 180
Capacitance	(uF)	12.7	12.3
Height	(mm)	60	45
Length	(mm)	78.9	78.9
Width	(mm)	20	20
Mass	(g)	164	160

These two actuators were chosen for their displacements of approximately 100 microns and force capabilities of over a 1000 newtons. The force capability of the actuators was sufficient for moving the loads related to the project of up to 100 pounds (445 newtons). The displacements produced by these actuators were desired to help achieve a high speed motor. For phase one of the project, the speed of the designed motor was the primary concern. Therefore, the APA120ML amplified actuator shown in Figure 2 was cho-

sen to be included as part of the design. The actuator was implemented into the design as a direct attachment between the two clamping mechanisms.

Figure 2. Cedrat Recherche's APA120ML.

The resulting assembled motor is shown in Figure 3.

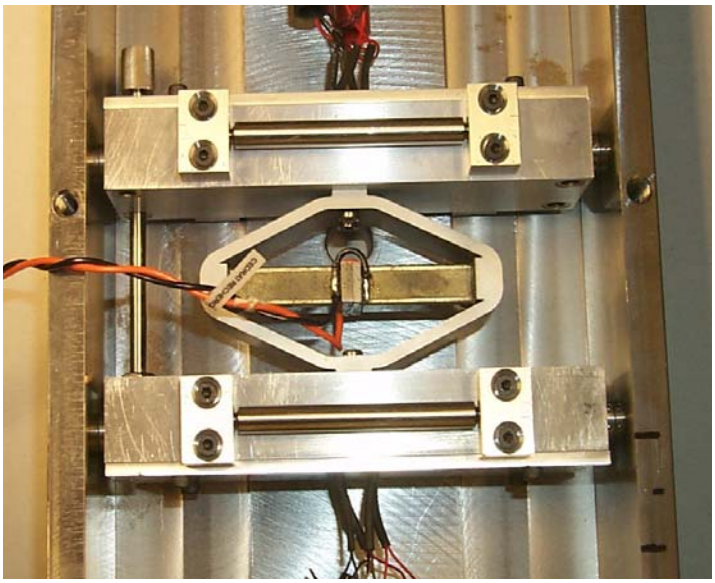

Figure 3. The phase one motor design.

Motor Model

A lumped-parameter model of the motor was developed to estimate its loaded and unloaded speed. The parameters chosen to be important for the designed motor were the stiffness and damping of the extending mechanism, the mass of the clamping mechanisms, the forces applied to the motor, and the forces generated by the motor. Using these motor parameters, a two degree of freedom (2DOF) mass-spring-damper system was used to model the motor's behavior. Note that the compliant amplified actuator used in this project actually contracts when activated. Figure 4 shows a diagram of the chosen model, where,

$M1$ = mass of Brake 1
$M2$ = mass of Brake 2
$X1$ = displacement of Brake 1
$X2$ = displacement of Brake 2
Ke_{act} = stiffness of extending actuator
C_{act} = damping coefficient of extending actuator
F_{act} = force generated by the extending actuator
F_{brake1} = frictional force of Brake 1
F_{brake2} = frictional force of Brake 2
$m \cdot g$ = force of applied load

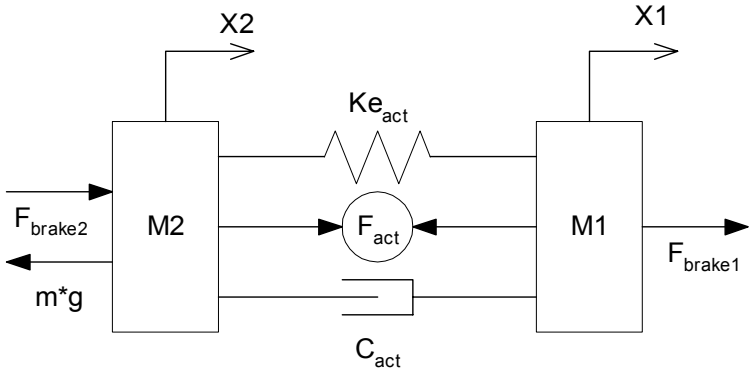

Figure 4. 2DOF model of motor.

To find the equations of motion for masses $M1$ and $M2$ a free body diagram for each mass was produced. By summing the forces the equations of motion were produced according to Newton's second law. The resulting equations of motion for $M1$ and $M2$ are shown in Equation 1 and Equation 2, respectively.

$$M1\ddot{X1} = -F_{ke} - F_C + F_{brake1} - F_{act} \quad (1)$$

$$M2\ddot{X2} = F_{ke} + F_C + F_{brake2} + F_{act} - m \cdot g \quad (2)$$

To explain what the forces shown in the equations of motion represent, a typical force equation for piezoelectric materials must be discussed. Equation 3 represents the force generated by a piezoelectric material. The force generated by a piezoelectric material (F_{gen}) can be represented by the product of the mass moved (M) and the acceleration ($\ddot{X}$) in which the mass moved. The force generated is the sum of an applied force (similar to F_{act}) minus a stiffness force (similar to F_{ke}) and a force due to damping (similar to F_C). The applied force is an result to an applied voltage (V) multiplied by a voltage constant (Kv), with the units N/V. The stiffness force is calculated as the product of the actuator's stiffness (Ke) and the displacement of the actuator (X). The force due to damping is calculated as the product of the damping coefficient (C) for the actuator and the velocity ($\dot{X}$) in which the actuator is moving. All of these calculations make use of parameters that are easily found using the manufacturer's specifications.

$$F_{gen} = Kv \cdot V - Ke \cdot X - C \cdot \dot{X} \tag{3}$$

Applying this knowledge to the forces shown in the equations of motion (Equations 1 and 2), the following force equations are produced

$$F_{act} = Kv_{act} \cdot V \tag{4}$$
$$F_{ke} = Ke_{act}(X1 - X2) \tag{5}$$
$$F_C = C_{act}(\dot{X}1 - \dot{X}2) \tag{6}$$

where,

Kv_{act} = voltage coefficient (N/V) of extending actuator
$\dot{X}1$ = velocity of Brake 1
$\dot{X}2$ = velocity of Brake 2

The force generated by the brakes is similar to Equation 3 with two exceptions. The damping force and the stiffness force do not apply, due to the assumption that motion is prevented when the brake actuators are activated against the solid walls of the guide channel. To find the frictional forces produced by the brakes the force generated by the brakes must be multiplied by a frictional coefficient (μ). In the simulation, both a static and dynamic friction coefficient were utilized to account for brake slippage. For the frictional forces created by both Brake 1 (F_{brake1}) and Brake 2 (F_{brake2}) the same equation can be used (Equation 7) with the individual brake parameters applied to the equation.

$$F_{brake} = \mu(Kv_{brake} \cdot V_{brake}) \tag{7}$$

where,

Kv_{brake} = voltage coefficient (N/V) of individual brake actuator
V_{brake} = voltage applied to individual brake actuator

The model presented previously in Figure 4 provides a representation of the designed motor which makes use of the provided manufacturer specifications for both the clamping actuators and the extending actuator. However, for this project is was desired to create a more detailed model that includes a representation of the internal components of the compliant amplified actuator. This more detailed model would allow the performance of the motor to be observed for any chosen internal parameter for the compliant actuator. The ability to observe the motor's performance for different internal parameters will prove to be helpful when deciding if an amplified actuator should be designed and built to meet the project's original goals, in phase two of the project. For the more detailed model shown in Figure 5 the compliant amplified actuator was broken down into two components: an internal PZT stacked actuator and a compliant amplifying structure. The internal PZT stacked actuator is represented by the model as an applied force (F_{pzt}) and a stiffness of Ke_{pzt}. The model presents the compliant amplifying structure as the stiffness K_{comp} and an amplification gain ($L2/L1$).

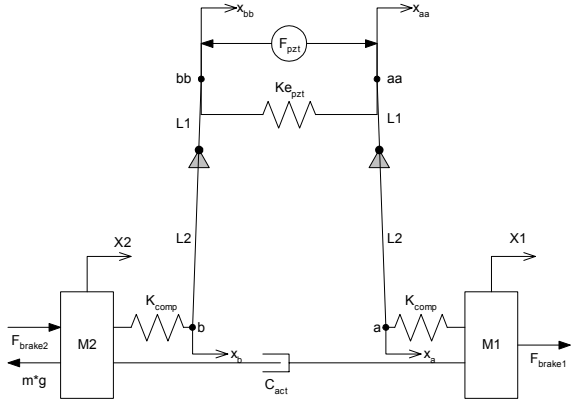

Figure 5. Detailed 2DOF model of motor.

where,

Ke_{pzt} = stiffness of PZT actuator used in amplified actuator

K_{comp} = stiffness of half the compliant amplifying structure
$L2/L1$ = gain of compliant structure
F_{pzt} = force generated by the PZT actuator used in the amplified actuator

Figure 5 can be related to the previous equations of motion (Equation 1 and Equation 2), by reducing the characteristics of the compliant amplified actuator to an equilvalent stiffness (Ke_{equ}) and an equivalent force (F_{equ}) as shown by the following equations. The equivalent force can be broken down into the product of an equivalent voltage coefficient (Kv_{equ}) and an applied voltage signal to the actuator (V_{act}).

$$M1\ddot{X}1 = -Ke_{equ}(X1-X2) - C_{act}(\dot{X}1-\dot{X}2) + F_{brake1} - F_{equ} \quad (8)$$

$$M2\ddot{X}2 = Ke_{equ}(X1-X2) + C_{act}(\dot{X}1-\dot{X}2) + F_{brake2} + F_{equ} - m\cdot g \quad (9)$$

To solve for the unknown equivalent stiffness (Ke_{equ}) and the equivalent voltage coefficient (Kv_{equ}) the model shown in Figure 5 was separated into six nodes: $M1$, $M2$, a, b, aa, and bb. A free body diagram was produced for each node to find the force equation represented at each node.

The resulting equations of motion were produced

$$M1\ddot{X}1 = -\left(\frac{K_{comp}Ke_{pzt}L1^2}{2\cdot Ke_{pzt}L1^2 + K_{comp}L2^2}\right)(X1-X2) - C_{act}(\dot{X}1-\dot{X}2) + F_{brake1} - \left(\frac{K_{comp}Kv_{pzt}L1\cdot L2}{2\cdot Ke_{pzt}L1^2 + K_{comp}L2^2}\right)V_{act} \quad (10)$$

$$M2\ddot{X}2 = \left(\frac{K_{comp}Ke_{pzt}L1^2}{2\cdot Ke_{pzt}L1^2 + K_{comp}L2^2}\right)(X1-X2) + C_{act}(\dot{X}1-\dot{X}2) + F_{brake2} + \left(\frac{K_{comp}Kv_{pzt}L1\cdot L2}{2\cdot Ke_{pzt}L1^2 + K_{comp}L2^2}\right)V_{act} - m\cdot g \quad (11)$$

where,

$$Ke_{equ} = \frac{K_{comp}Ke_{pzt}L1^2}{2\cdot Ke_{pzt}L1^2 + K_{comp}L2^2} \quad (12)$$

$$Kv_{equ} = \frac{K_{comp}Kv_{pzt}L1\cdot L2}{2\cdot Ke_{pzt}L1^2 + K_{comp}L2^2} \quad (13)$$

These detailed equations of motion (Equations 10 and 11) were assembled into a SIMULINK model. The SIMULINK block diagram will simulate the motor's behavior for the chosen parameters and input signals. The corresponding MatLab files used to define values for the motor parameters and to determine whether Brakes 1 or 2 were stationary or slipping. The SIMULINK simulation parameters were chosen to make use of an ODE23t ordinary differential equation solver and a tolerance of 0.001.

Motor Performance and Model Verification

For the results presented in this section, the amplifier used to control the extender was limited to a maximum output voltage of 130 volts. The amplifier also limited the waveform input to the extender to a square wave approximation. It should be noted that the voltage limitation reduced the maximum displacement of the extender, thus reducing the velocity of the motor.

Experimental Setup

The setup used to test the performance of the designed motor is shown in Figure 6. First, the motor was placed into the guide channel and the adjustable interfaces were adjusted to minimize the clearance between the clamping interface and the guide channel. Using the Dspace DSP the desired control signals for each component of the motor were created. These signals were sent through three separate amplifiers to achieve the desired voltage signal at each of the motor's components. While the motor was running, the Dspace DSP recorded the motor's displacement as function of time from the Polytec Laser Vibrometer.

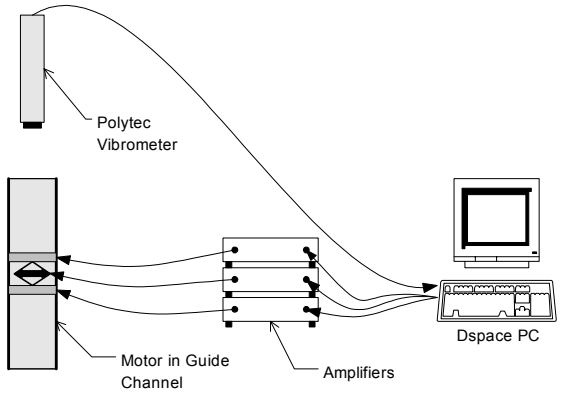

Figure 6. Experimental setup to run the motor.

Unloaded Case

For the unloaded case, a comparison was conducted between the experimental and model results at a cycle rate of 10 Hz. In Figure 7a the comparison shows that the modeled results closely matched the experimental results. The comparison found that the modeled simulation produced a displacement of 0.3 millimeters less than the experiment over a time of 10 seconds, a difference in velocity of 0.03 mm/sec. To observe the differences between the results a cutaway view of the comparison is presented by Figure 7b. In the cutaway view the reason for the modeled simulation's underestimate is revealed. At low frequencies "creep" affects the experimental results by increasing the step size. "Creep" as shown in Figure 7b, is the small increase in displacement of an activated PZT stack as time goes on [Physik_Instrumente (1998)]. As drive frequencies increase the effect of creep on experimental results will be less evident.

From observing the cutaway view, one can also notice that the experimental results demonstrated much more damping than the modeled simulation. One reason for the difference can be attributed to the input signal to the extender. The input square wave approximation produced by the amplifier was similar to a true square wave with the activation and deactivation slopes comparable to the first half of a sine wave and the later half of a sine wave, respectively. Therefore, the input signal gives the appearance of a damped response. Another reason for the difference, was the increased damping due the friction between the guide channel and clamping interface during forward movement. For phase one the project this difference in damping did not drastically affect the modeled simulation, so the modeled damping was left equal to the damping of the extending actuator (C_{act}).

The resulting performance of the linear motor for an unloaded case found that a speed of 4.9 mm/sec could be produced for a max voltage input of 130 volts at 50 Hz. The model slightly overestimated the result to be 5.4 mm/sec. A summary of the unloaded results is shown in Figure 8. Using the model the predicted performance of the motor using the full voltage input to the extender (180 V) at 50 Hz was found to equal 7.5 mm/sec.

Loaded Case

For the loaded case, a comparison was conducted between the experimental and model results of moving a 9.1 kilogram (20 lbs) load at a cycle rate of 10 Hz. The model simulation predicted the motor would move 6.7 mm in seven seconds, when in actuality the motor moved 5.2 mm in seven seconds. An average loss of approximately 21 microns per cycle was unaccounted for by the model. To better understand what caused these additional losses a closer look was taken at the experimental results.

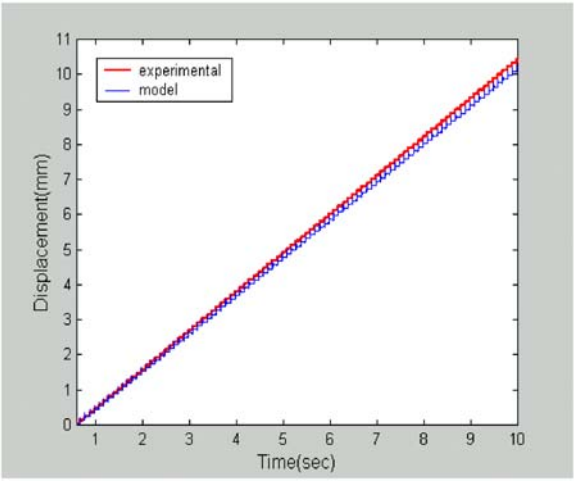

Figure 7a. Experimental to model comparison for an unloaded motor.

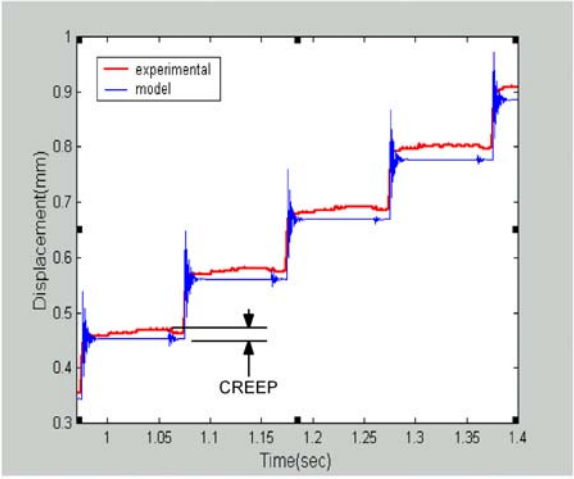

Figure 7b. Cutaway view of comparison.

A closer look at the experimental results found both consistent and inconsistent losses. To help explain the losses a summary of typical loaded cycles is shown in Figure 9b. The inconsistent losses occurred at the points in time 2 and 3. At point 2 the inconsistent loss occurred when Brake 1 was activated and Brake 2 was deactivated. The loss produced was assumed to be a result of the clearances between the cylindrical button interfaces and their supporting bushings of Brake 1. For point 3 the losses occurred when the extender was activated pulling Brake 2 and the load forward. Initially it was felt that the losses at this point was due to slipping at the interfaces. However, the fact that losses at point 2 and 3 were never seen in the same cycle lead to a different conclusion. The conclusion found that when a loss

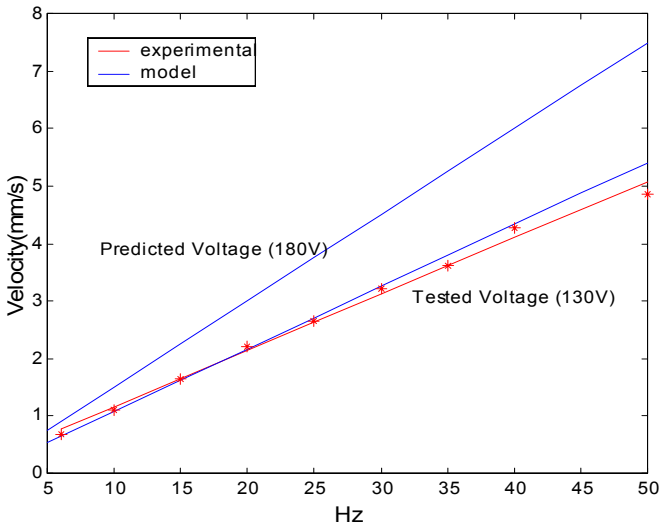

Figure 8. Velocity vs. Frequency for designed motor.

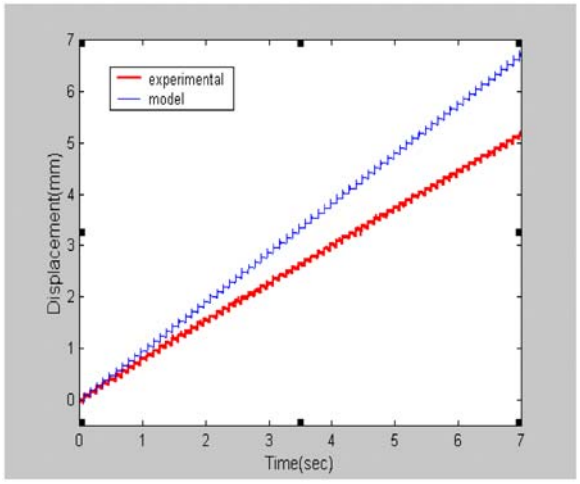

Figure 9a. Experimental to model comparison for the loaded motor.

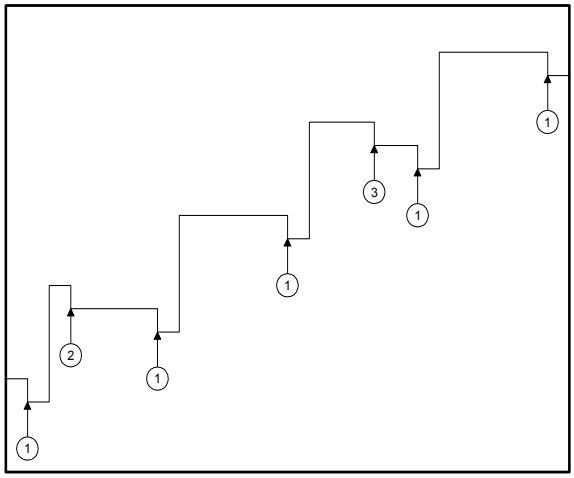

Figure 9b. Losses due to loading.

did not occur at point 2 due to button interface clearances, occasionally at point 3 the loss due to button interface clearances would appear. Neither the loss at point 2 or at point 3 was guaranteed to occur during every cycle. However, the frequency in which the losses occurred increased with load. Due to the unpredictability of these losses it was difficult to accurately model the losses. Therefore, in phase one of the project the inconsistent losses were not included in the model. At point 3 consistent losses occurred when Brake 2 was activated and Brake 1 was deactivated. The model takes in account the losses due to a loaded/unloaded condition at this point; however, additional losses were found evident. These additional losses were assumed to be a result of the clearances between the cylindrical button interfaces and their supporting bushings of Brake 2. The consistency of the losses at point 3 allowed the losses to be included in the model simulation.

To improve the performance predicted by the model, the stiffness of the compliant structure was reduced to match the consistent losses. The fact that the consistent losses appeared at the same time as the loading losses, allowed a reduction in stiffness of the compliant structure to match the experimental results. By reducing the compliant structure stiffness the possible step size produced by the actuator will be maintained. However, the force produced by the actuator will be reduced and the rise time will be increased. Since phase one of the project only looks at low frequencies (below 50 Hz), this reduction in stiffness will work well. To predict the motor's loaded performance at higher frequencies the method used to account for the consistent losses will have to be changed. Using the improved model the comparison between the model simulation and experimental was produced again. The improved model simulation predicted the motor would move 5.5 mm in seven seconds, when in actuality the motor moved 5.2 mm in seven seconds. A result was an improved average of unaccounted losses from approximately 21 microns to 4 microns per cycle. The model simulation still over estimated the experimental results due to the erratic losses, but produced relatively similar results for small loads, less that 9.1 Kg (20 Lbs).

To summarize the results for the loaded case a velocity verses load plot is shown in Figure 10. Ideally the model simulation shows that the loss in velocity due to loading should have a linear relationship. In actuality the rate of the loss in velocity increased as the loading increased. This was

an immediate result of the regularity in the erratic losses increasing as the load increased. The experimental results of the loaded case were extrapolated to find that the phase one design has a stall load of approximately 17 kilograms (38 lbs).

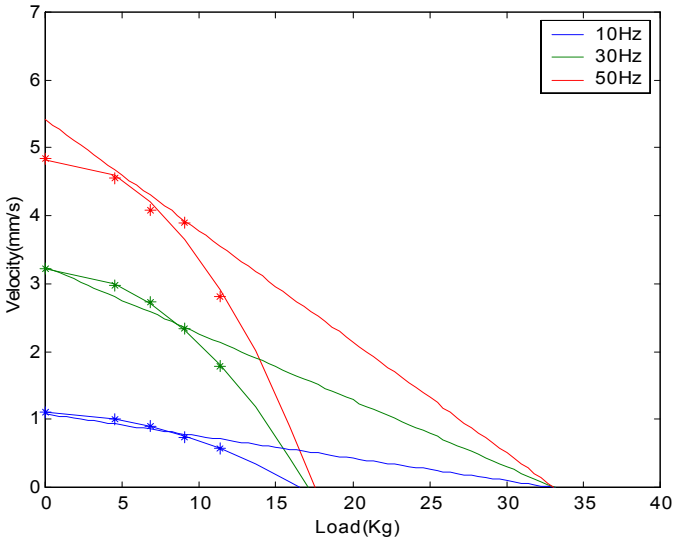

Figure 10. Speed vs. Load for designed motor.

Power Characteristics

To create a more efficient motor, the power characteristics of the initial motor design were investigated. The mechanical power output of the motor as a function of load was examined to find the operating conditions that produced the peak motor performance. The power necessary the drive the motor was assessed to find how the operating conditions affected the driving power.

Mechanical Power The output performance of the linear motor can be characterized by the mechanical power the motor can produce. The mechanical power can be found simply by the product of the load force and the average velocity of the motor. In Figure 11 the mechanical power output is shown as a function of load for cycle frequencies of 10, 30, and 50 hertz. The results found that the peak performance of the motor occurred under a load of approximately 100 newtons [23 lbs] and increased as the cycle frequency increased. The peak mechanical power produced by the motor was 310 mW corresponding to an average velocity of 3.1 mm/sec.

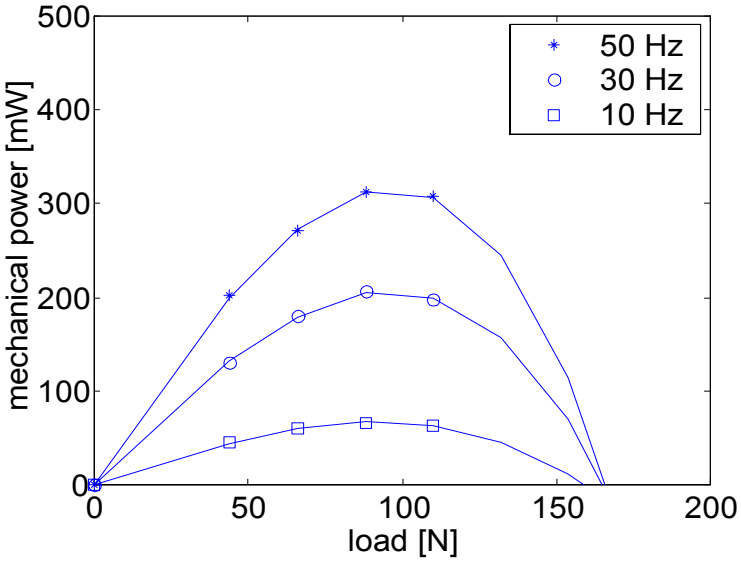

Figure 11. Mechanical power output as a function of motor load.

Driving Power The power necessary to drive a piezoelectric linear motor can be found by the product of drive voltage (V_{drive}) and the drive current (I_{drive}). Due to the fact that piezoelectric materials behave similar to capacitors, the drive current can be represented by Equation 14. The equation shows that the amount of capacitive material used to create the motor will determine the current necessary to drive the motor.

$$I_{drive} = C\frac{dV_{drive}}{dt} \tag{14}$$

To test the power consumption of the motor, a switching amplifier used to power the extending actuator throughout the project was utilized. The switching amplifier has the limitation of a set output waveform. However, switching amplifiers are found to be much more efficient than linear amplifiers when driving capacitive loads. The switching amplifier is designed specifically for the application of driving capacitive material. Due to its design the amplifier is able to utilize the regenerative current produced by piezoelectric materials. The result is that there the amplifier supplies power to activate the actuator and the actuator returns a regenerative power back to the amplifier when deactivated. Therefore, the power consumed by the actuator is the difference between the power supplied and the regenerative power produced.

The results for the braking mechanisms found that an average power of 7.7 Watts was supplied to the actuator and

average power of 3.3 Watts was consumed by the actuator at 50 Hz. The extending mechanism required a supplied power of 14.3 Watts and consumed an average power of 6.1 Watts at 50 Hz. The results of the extending mechanism also show that the loading of the extending mechanism had little affect on the average power required to run the motor. Overall, the motor consumed an average power of 12.7 Watts at a drive frequency of 50 Hz.

CONCLUSIONS

The piezoelectric incremental motor design produces a stall load of approximately 17 kg and an unloaded velocity on the order of 5 mm/sec when operated at 50 Hz. The primary limitations to improving the performance were the limitations in the amplifier output current and erratic losses attributed to clearance problems in the brake mechanism. Our analysis also demonstrated that the efficiency of the motor was on the order of only 2% when comparing the average mechanical power output to the average electrical power input.

REFERENCES

A. Hara, T. Horinchi, K. Yamada, S. Takahashi, and K. Nakamura, 1986, "Electomechanical Translation Device Comprising an Electrostrictive Driver of a Stacked Ceramic Capacitor Type," Patent #4,570,096.

A.D. Brisbane, 1968, "Position Control Device," Patent #3,377,489.

B. Edinger, M. Frecker, and J. Gardner, 1999, "Dynamic Modeling of an Innovative Piezoelectric Actuator for Minimally Invasive Surgery," Adaptive Structures and Materials Systems (ASME), vol. 59, pp. 183–188.

B. Zhang and Z. Zhu, 1994, "Design of an Inchworm-Type Linear Piezomotor," SPIE Proceedings, vol. 2190, pp. 528–539.

Cedrat_Recherche, 2000, "Piezo Actuators Catalogue," Version 2.1.

C.G. O'Neill and C.E. Foster, 1980, "Electromotive Actuator," Patent #4,219,755.

G. Carman, Q. Chen, D. Yao, and C. Kim, 1999, "Mesoscale Actuator Device: Micro Interlocking Mechanism to Transfer Macro Load," Sensors and Actuators, vol. 73, pp. 30–36.

Galante, T., 1997, "Design and Fabrication of a High Authority Linear Piezoceramic Actuator: The PSU H3 Inchworm," Master's thesis, The Pennsylvania State University.

G.L. Locher, 1967, "Micrometric Linear Actuator," Patent #3,296,467.

G.R. Stibitz, 1964, "Incremental Feed Mechanisms," Patent #3,138,749.

G.V. Galutva, 1972, "Device For Precision Displacement of a Solid Body," Patent #3,684,904.

J. Frank, G. Koopmann, W. Chen, and G. Lesieutre, 1999, "Design and Performance of a High Force Piezoelectric Inchworm Motor," SPIE Proceedings, vol. 3668, pp. 717–723.

J. Oliver, R. Neurgaoukar, J. Nelson, and C. Bertolini, 1998, "Moving Linear Piezoelectric Motor for Vehicle Appications," Patent #5,780,957.

J.E. Miesner and J.P. Teter, 1994, "Piezoelectric/Magnetosrictive Resonant Inchworm Motor," SPIE Proceedings, vol. 2190, pp. 520–527.

Physik_Instrumente, 1998, "NanoPositioning," Catalog # 114.

R.A. Bizzigotti, 1975, "Electromechanical Translation Apparatus," Patent #3,902,085.

S. Canfield, B. Edinger, M. Frecker, and G. Koopmann, 1999, "Design of Piezoelectric Inchworm Actuator and Compliant End-Effector for Minimally Invasive Surgery," SPIE Proceedings, vol. 3668, pp. 835–843.

S. Hsu, A. Arbor, and A. Blatter, 1966, "Transducer," Patent #3,292,019.

S. Lee and M. Esashi, 1995, "Design of the Electrostatic Linear Microactuator Based on the Inchworm Motion," Mechatronics, vol. 5, pp. 963–972.

T. Fujimoto, 1988, "Linear Motor Driving Device," Patent #4,736,131.

T. Murata, 1990, "Drive Apparatus and Motor Unit Using The Same," Patent #4,947,077.

T. Pandell and E. Garcia, 1996, "Design of a Piezoelectric Caterpillar Motor," Proceedings of the ASME Aerospace Division, vol. 52, pp. 627–648.

T. Shibuya, 1988, "Piezoelectric Motor," Patent #4,777,398.

W.G. May, Jr., 1975, "Piezoelectric Electromechanical Translation Apparatus," Patent #3,902,084.

Z. Zhu and B. Zhang, 1997, "Developing a Linear Piezomotor With Nanometer Resolution and High Stiffness," IEEE/ASME Transactions on Mechatronics, vol. 2, pp. 22–29.